Cardiac CT: Contemporary Clinical Image Data Display, Analysis, and Quantification

13

Moritz H. Albrecht, Marwen Eid, and Pal Spruill Suranyi

Why Do We Need "Advanced Visualization" and Quantification?

One of the most significant breakthroughs in cardiac CT imaging was being able to acquire isotropic resolution datasets with sufficient temporal resolution to take "snapshots" of this dynamic, ever-moving organ. Isotropic three-dimensional (3D) datasets acquired with either prospective triggering or retrospective gating, and further complicated by the dimension of time within the cardiac cycle, effectively yielding four-dimensional (4D) datasets, allow for a variety of post-processing techniques useful for advanced visualization of cardiovascular anatomy and pathology. Some of these techniques are fancy, colorful, and eye-pleasing or just serve as an aid to student or patient education, but others have become a crucial part of our clinical routine when evaluating cardiac CT images and discussing findings with non-radiology physicians.

Secondly, in the era of "precision medicine" and "imaging biomarkers," it is paramount to strive for more quantitative analysis of our findings. Thus, teasing out objective numbers and values from our large datasets is becoming increasingly important. Initially calcium scoring was the pioneer in quantitative cardiac evaluation. Since then various workstations and algorithms have been developed for routine clinical use to measure myocardial mass and function, to evaluate cardiac chamber sizes, and to assess coronary plaques and stenoses.

Lastly, as we are striving to understand the correlation between pathophysiology, qualitative and quantitative image findings, and patient outcomes, multiple investigational methods are still being developed, holding the promise of future clinical utility for myocardial perfusion imaging and analysis of coronary hemodynamics. In this chapter, we will briefly touch on each of these methods and will try to elucidate their diagnostic value and potential future clinical implementation.

Clinical Image Data Display and Analysis

3D Volume Rendering Techniques (VRT)

Although initially developed by the animation movie industry, 3D VRT reconstructions have been rapidly adopted in clinical medical imaging [1]. While the exact technical details are beyond the scope of this chapter, the general idea is that interactive probability-based algorithms and workstations build virtual 3D models of an organ using the 3D matrix of enhancement values by deciding whether a given volume element, i.e., voxel, belongs to an adjacent structure or not.

To stay on focus, this chapter will include all of these techniques under the umbrella of 3D VRT. However, it should be noted that there are fine nuances differentiating the various surface rendering techniques, e.g., shaded realistic surface displays (Fig. 13.1), and volume rendering approaches which can be further manipulated to generate fly-through or fly-around views of various organs [2]. Using creative display colors for different tissue types as well as various lighting methods and depth shading, these techniques enable the analysis of a dataset from any desired angle, including from within the vessel lumen. By changing the attenuation level-based visualization thresholds, one can hide or accentuate certain organs and tissue types or even make them semitransparent. In order to simplify the selection

M. H. Albrecht
Department of Diagnostic and Interventional Radiology, University Hospital Frankfurt, Frankfurt am Main, Germany

M. Eid
Division of Cardiovascular Imaging, Department of Radiology and Radiological Science, Medical University of South Carolina, Charleston, SC, USA

P. S. Suranyi (✉)
Division of Cardiovascular Imaging, Department of Radiology and Radiological Science, Medical University of South Carolina, Charleston, SC, USA

Division of Cardiology, Department of Medicine, Medical University of South Carolina, Charleston, SC, USA
e-mail: suranyi@musc.edu

U. J. Schoepf (ed.), *CT of the Heart*, Contemporary Medical Imaging, https://doi.org/10.1007/978-1-60327-237-7_13

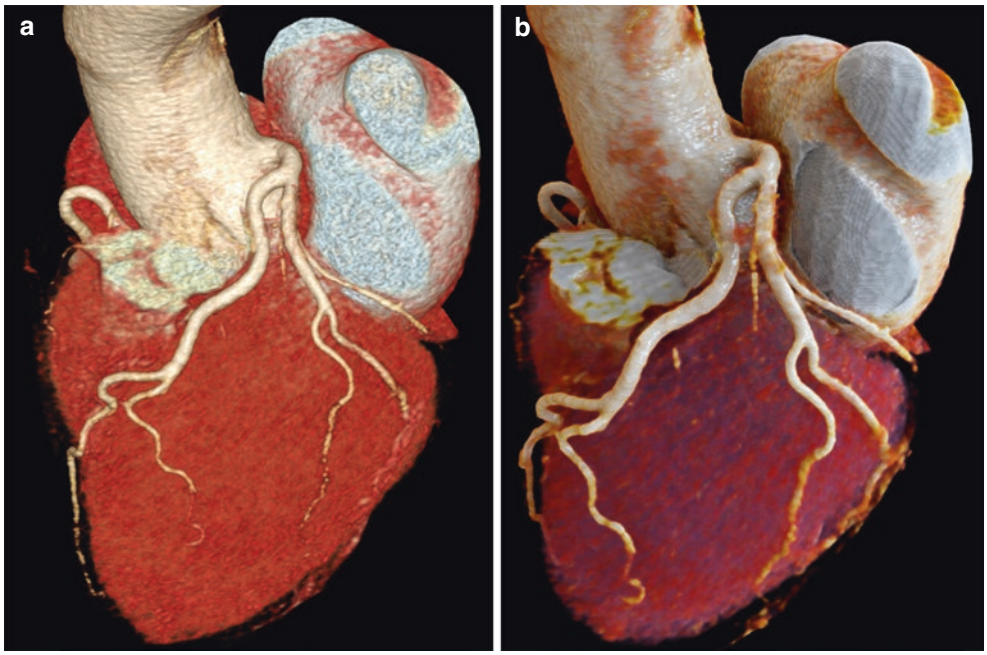

Fig. 13.1 Several approaches exist for 3D visualization of the heart and coronaries. While traditional 3D volume rendering technique (VRT) images (**a**) facilitate the orientation and anatomical relations to adjacent organs, novel cinematic rendering (**b**) allows furthermore for a photo-realistic appearance and analysis of the organ surfaces

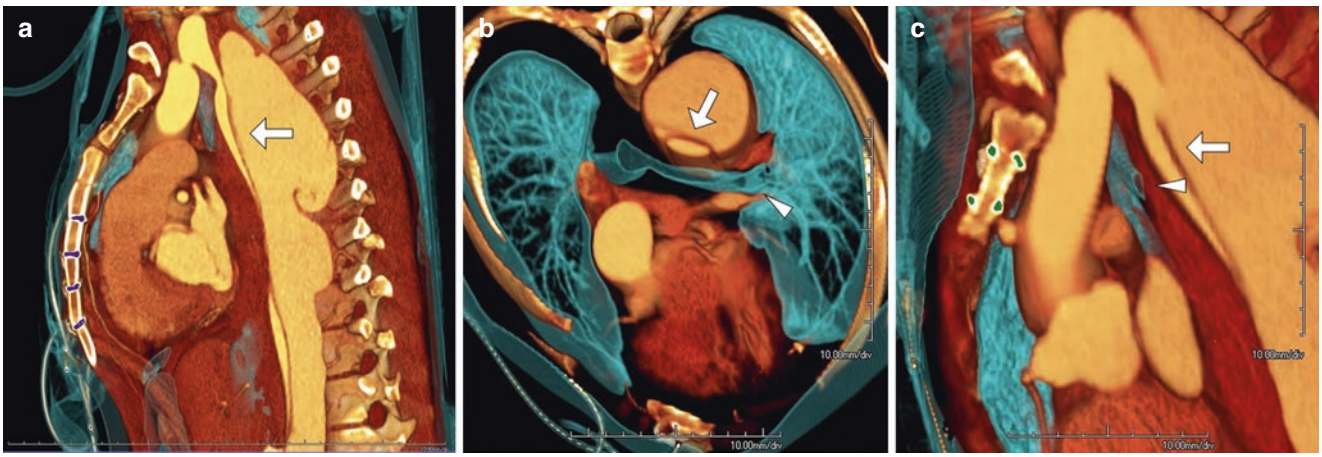

Fig. 13.2 3D reconstruction images displaying the utility of 3D VRT images in a patient with Marfan syndrome with prior history of ascending aorta repair (note sternal wires highlighted in purple, **a**), presenting with acute chest pain and shortness of breath. The sagittal image (**a**) shows a type-B aortic dissection (*arrow*). The oblique axial (**b**) and sagittal (**c**) images show the aneurysmal descending aorta (*arrow*) compressing on the left main bronchus (*arrowhead*). The various tissue types and metallic sternal wires can be clearly delineated by assigning different colors based on CT attenuation enabling us to demonstrate the relationship of airways to great vessels and the proximity of anterior structures to sternal wires

of the best technique for a given indication, workstations have presets stored for various purposes which often require further interactive manual adjustment by the reader.

Volume rendering of the heart and adjacent anatomic structures is helpful to obtain an overall understanding of the spatial relationship between organs, airways, the chest wall, and vascular pathologies (Fig. 13.2). 3D VRT is also beneficial in providing an overview of the quality of our datasets, especially in the case of arrhythmias or misregistrations, also called "step-offs," which can be easily spotted in a 3D view.

When emphasizing vessels, however, one must understand that the goal of contrast media administration in cardiac CT is to improve the visualization of the vascular lumen rather than its surface. Also, when analyzing vessels with stents, 3D VRT shows the presence of the stent but does not show its content. Thus, 3D VRT cannot determine whether a stented vessel lumen is patent, occluded, or if it has intimal hyperplasia.

Further shortcomings of 3D VRT include locating the presence of calcifications, which may appear to be located on the surface of the vessel when in fact they are in the vessel wall. It is also important to note that motion artifacts and

streak artifacts may cause artifactual vessel stenosis on 3D VRT, which may be misleading for beginners in cardiac CT. Therefore, experts do not recommend making diagnoses solely based on VRT reconstructions but advise using 3D VRT as an auxiliary technique to supplement standard cross-sectional images when making a diagnosis.

Automated, Semiautomated, or Manual Segmentation of the Heart

Sophisticated workstations offer the option for automatic segmentation of the heart, which virtually "removes" the ribcage and the lungs to allow for 360-degree visualization of the heart's chambers and vessels. Such automated segmentation simplifies the visualization of routine cases, but semiautomated or manual segmentation is preferred when trying to analyze more challenging postsurgical cases or patients with unusual anatomies.

Unfortunately, automated segmentation algorithms may "remove" venous bypass grafts, the internal mammary arteries, or parts thereof, which may lead to the erroneous diagnosis of occluded bypass grafts. Similarly, human observers may inadvertently "remove" vessel segments or create "nicks" in vessels during post-processing when generating the volume-rendered segmented heart, thus causing potential problems for interpretation. This is why most experts strongly emphasize looking at the "source images" whenever a 3D VRT image suggests abnormal pathology.

The alternative to segmenting out the heart is to look at the entire 3D dataset using a cut plane or a slab, which allows the user to scroll through the organs in the chest in 3D while also making sure that no structures remain hidden due to erroneous segmentation (Fig. 13.3).

Dedicated Cardiac Planes, MPR, and Thick-MPR

Multi-planar reformatting (MPR) images represent the standard cross-sectional reconstructions in cardiac CT. A 3D or 4D dataset with essentially isotropic resolution allows one to arbitrarily choose the ideal plane when studying the heart. Whether it is one of the standard long- and short-axis planes (Fig. 13.4) or a more dedicated view such as one showing the aortic valve leaflets or any other structure of interest, this can be performed at a workstation in a matter of seconds using MPR of the original source imaging data. Thus, a "simple" MPR image shows the reconstructed data in arbitrary non-axial planes with a thickness of one voxel. These views are useful in performing anatomic measurements in vessels or valves or within the chambers.

Most workstations also offer the option of generating "thick-MPRs," which consist of virtually thickened CT slices that improve the signal-to-noise ratio in compromised datasets and help visualize structures that may be moving in and out of the imaging plane during the cardiac cycle (e.g., aortic valve). Furthermore, thick-MPRs are also useful if structures have both high- and low-density components, e.g., a sclerotic aortic valve with superimposed vegetation or thrombus (Fig. 13.5).

Curved MPR, Stretched MPR, and MAR

The basic principle of curved MPR (cMPR) is similar to that of linear MPR in that it uses the reconstructed dataset without additional manipulation of the Hounsfield units (HU) but still allows for the close-up analysis of vessels. The key feature of cMPR is the "centerline," which is either automatically or semiautomatically predetermined. Subsequently, the dataset is reformatted with resulting images showing data that is perpendicular to this centerline. It is paramount that the centerline should go through the vessel lumen, because otherwise the vessel may appear artifactually stenosed. Thus, before actually examining the cMPRs, one must carefully check – and if needed, adjust – the centerline. Normally there are two cMPR images displayed next to each other, where one is perpendicular to the other and both are perpendicular to the centerline. This dataset can then be manually "swiveled" about the centerline to look at all possible aspects of a vessel and take a closer look at any particular vessel segment of interest (Fig. 13.6).

In this context, it is important to emphasize the relevance of the window/level settings when studying vessels with stenosis, especially with the presence of calcifications or implanted stents. The apparent size of the calcified lesions greatly depends on the window/level settings, as shown in Fig. 13.7. Therefore, when stents or calcifications are present and cause blooming artifacts, it is important to take a second look at the vessel after "darkening" the image prior to making a diagnosis. This can be achieved by widening the window settings, which reduces the influence of blooming artifacts that can potentially lead to an overestimation of luminal narrowing.

A second caveat to remember is that stents and calcified vessel segments are better evaluated using a sharper reconstruction kernel and iterative reconstruction techniques. Unfortunately, these need to be applied at the time of reconstructing the axial datasets from the raw imaging data [3] (Figs. 13.8 and 13.9).

Another capability of the above technique is that the centerline's natural curves can be virtually stretched, resulting in sMPR images ("s" for stretched or straight). However, some experts consider this method too unnatural and vulnerable to over manipulation. Additionally, multiple aligned reformats can be generated by combining the cMPRs of multiple vessels. This technique uses

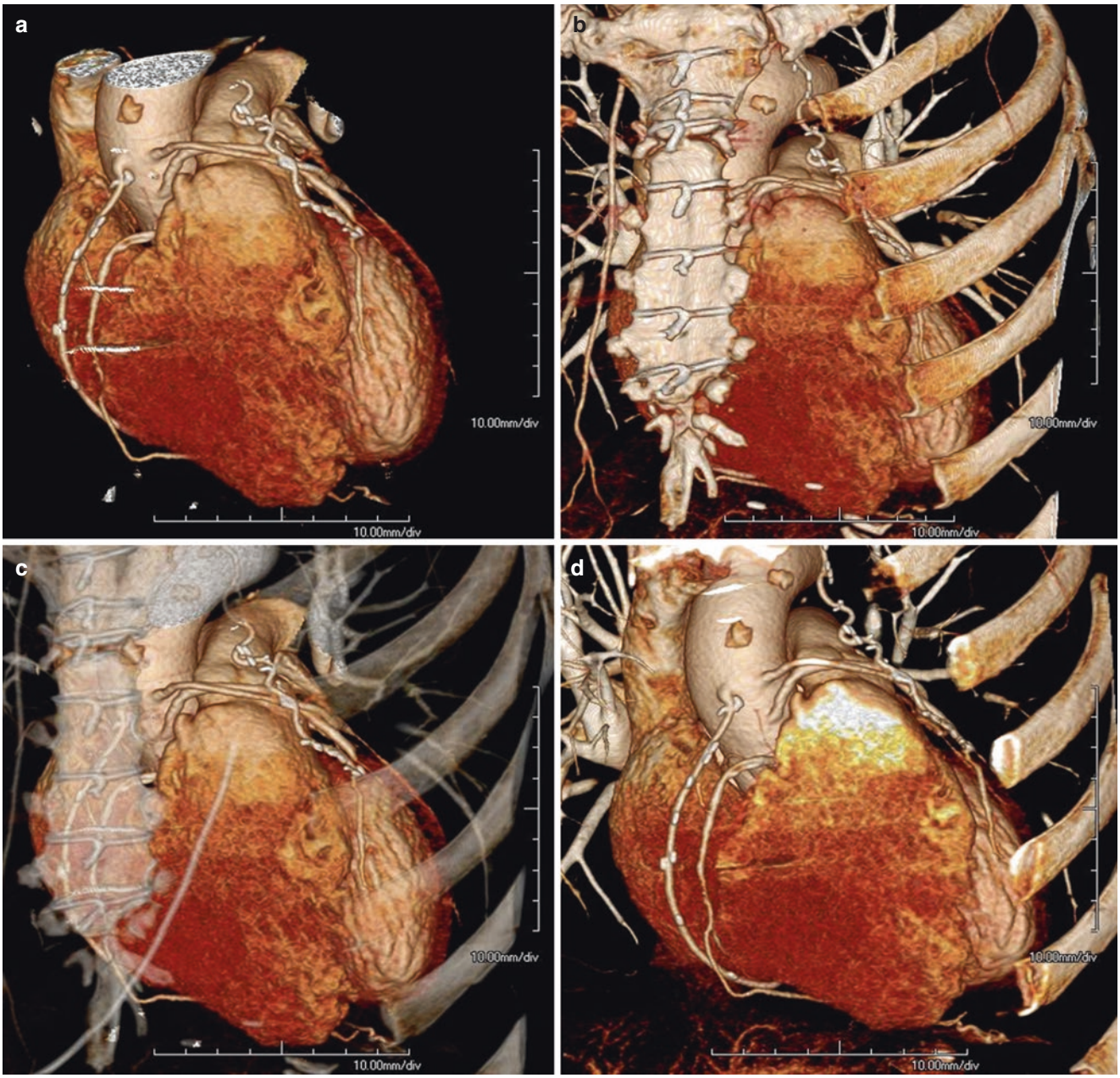

Fig. 13.3 3D reconstruction of the heart in a patient after coronary arterial bypass graft (CABG) surgery. The heart can be automatically segmented (**a**) and isolated from the remaining structures; however, this technique sometimes artificially removes important parts of the anatomy, like the proximal aspect of the LIMA graft in this case. Unfortunately, the heart and grafts cannot be seen in their entirety on the full volume either, due to overlying ribs and sternum. (**b**) The solution is a semitransparent (**c**) rib cage or a clip plane/slab, which both can visualize structures obscured by the chest wall (**d**), without losing information, thus reducing the likelihood of misinterpretation

the same principles as cMPR but aims to depict several vessel paths simultaneously by taking into account the multiple centerlines of multiple vessels. This technique provides an overview of the coronary anatomy and may prove useful in planning the placement of multiple stents near bifurcations.

The efficient segmentation of the coronary tree can provide us with a quick overall understanding of the blood supply routes of the myocardium. The coronary tree may then be projected onto polar maps of regional function or perfusion (Fig. 13.10), which has the added benefit of being able to "pair" vessel-specific stenosis with corresponding regional myocardial dysfunction or perfusion abnormality.

Projection Techniques

Maximum and minimum intensity projections are obtained when a 3D slab of the original reconstructed dataset is taken (more than one voxel in thickness) and a single two-

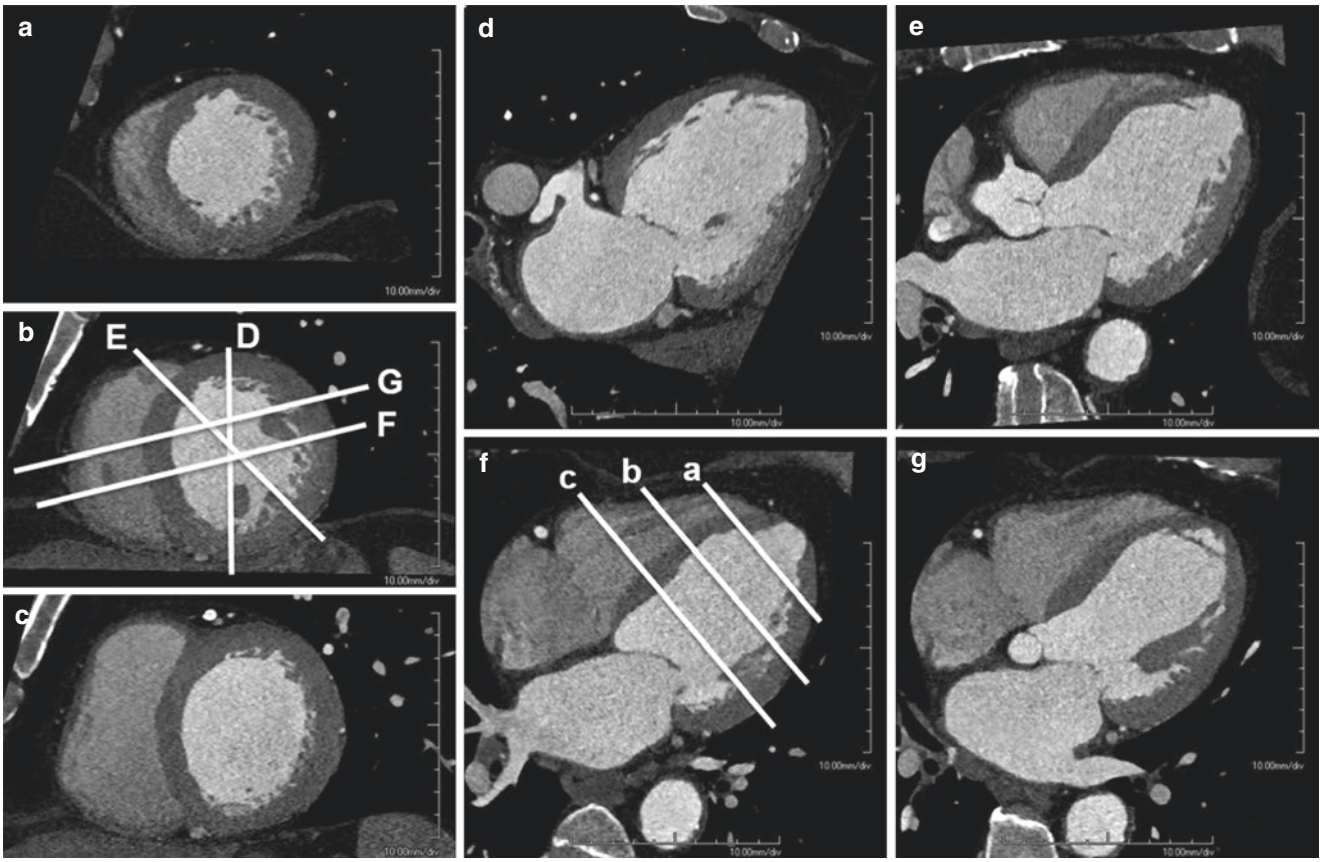

Fig. 13.4 This figure shows the standard planes for cardiac CT evaluation. As the cardiac axis is highly variable in every individual, conventional radiological axial, sagittal, and coronal images are not optimal for assessment of the heart. Manual adjustment on a 3D workstation is necessary to define true long and short axes of the heart. The spatial correlation among the short-axis (**a**, apical; **b**, mid; **c**, basal), 2-chamber (**d**), 3-chamber (**e**), 4-chamber (**f**), and 5-chamber views (**g**) is demonstrated here by white reference lines

dimensional image is generated. This can be performed by either taking only the lowest (minimum intensity projection (MINIP)) or only the highest attenuation (maximum intensity projection (MIP)) across the slab. An additional technique called average intensity projection (AIP), also called "thick-MPR" as previously described, uses the average attenuation values of all voxels across the slab.

MIP

Thin (<10 mm) and thick (>10 mm) MIPs are most useful for the assessment of vessels or bypass grafts when the contrast medium-filled lumen is of high interest. MIPs facilitate the tracking of the vessel paths, bifurcation analysis, and the evaluation of the length of stenotic segments. It is worth mentioning that some workstations have the capability to generate curved MIP images (cMIP), which uses the same principles as cMPR except that the end result is a MIP that is perpendicular to the centerline throughout the length of a given vessel. Although MIP is very useful for the aforementioned purposes, care must be taken when using it to assess the severity of vessel stenosis due to its potential to mislead the observer and cause over- or underestimation of stenosis. Thus, for the quantification of stenosis, it is most appropriate to use either the source images or cMPR images. An additional shortcoming of only using MIPs is the potential to "miss" low-density lesions such as small emboli, intimal flaps, abnormal valve apparatus (e.g., ruptured chordae), or even myocardial hypoattenuation.

MINIP

When the structures of interest are of low attenuation, it is helpful to use MINIPs, which may reveal pathologies that would be too subtle, if not invisible when using MPRs or MIPs. Examples include ischemic regions of the myocardium, infarcted areas, fatty infiltration of the myocardium, valves, chordae tendineae, papillary muscles, vegetations, thrombi or dissection membranes, and even airways. Figure 13.11 provides an example where MINIP, MPR, and MIP are compared side by side.

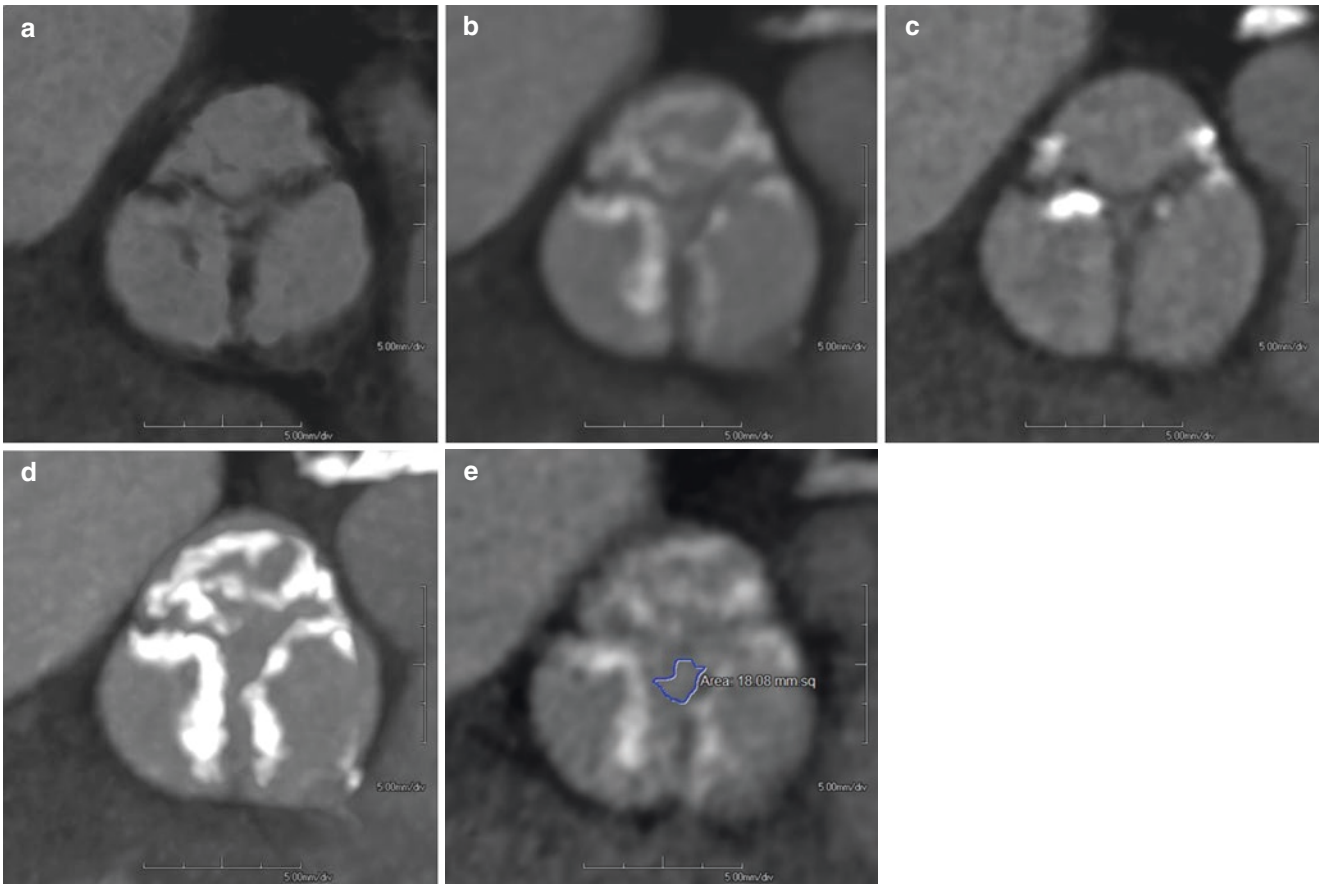

Fig. 13.5 Varying cross-sectional visualization techniques lead to different depictions of a calcified and stenotic aortic valve. (**a**) Minimum intensity projection (MINIP), showing only low-density portions of the valve. (**b**) Thick multi-planar reformat (thick-MPR) shows all portions of the valve but is blurry due to volume averaging. (**c**) Standard MPR, with high spatial resolution, does not show the entirety of the valve and the true extent of disease. (**d**) Maximum intensity projection (MIP) highlighting calcifications but hiding noncalcified portions of the valve. (**e**) Valve orifice measurement on the thick-MPR

Quantification

In addition to the relatively well-established contemporary clinical image data display and analyzing techniques, the field of objective image quantification is rapidly growing and represents the most investigated topic in state-of-the-art cardiac CT.

Calcium Scoring

Coronary artery calcium scoring, also known as Agatston scoring, is the most validated method for the prediction of patient outcome and risk stratification and has substantially enhanced the utility of cardiac CT imaging. In a standardized fashion, the Agatston score is semiautomatically calculated based on two parameters: the area of calcified coronary plaques with an attenuation greater than 130 HU on an ECG-synchronized noncontrast cardiac CT and a density factor which is based on the maximal attenuation of the same plaque. Using an online calculator based on the Multi-Ethnic Study of Atherosclerosis (MESA) study (https://www.mesa-nhlbi.org/Calcium/input.aspx), patients can be assigned to standardized risk categories with a low user-dependent variability compared to purely subjective or qualitative CT analysis. More advanced quantitative methods include calcium volume and density scores, and the hope is that fully automated Agatston scoring may be available in the near future [4]. Further details regarding Agatston scoring are discussed in another chapter of this book.

Coronary Stenosis Quantification/Fractional Flow Reserve

Workstations have evolved to the point where algorithms based on attenuation levels within the coronary lumen allow us to quantitatively evaluate vessel stenosis [5, 6]. Currently, this is performed in a semiautomated fashion in which the observer defines the segment of interest by placing a mark just proximal to the starting point of the plaque and another just beyond the distal end of the plaque using cMPR images

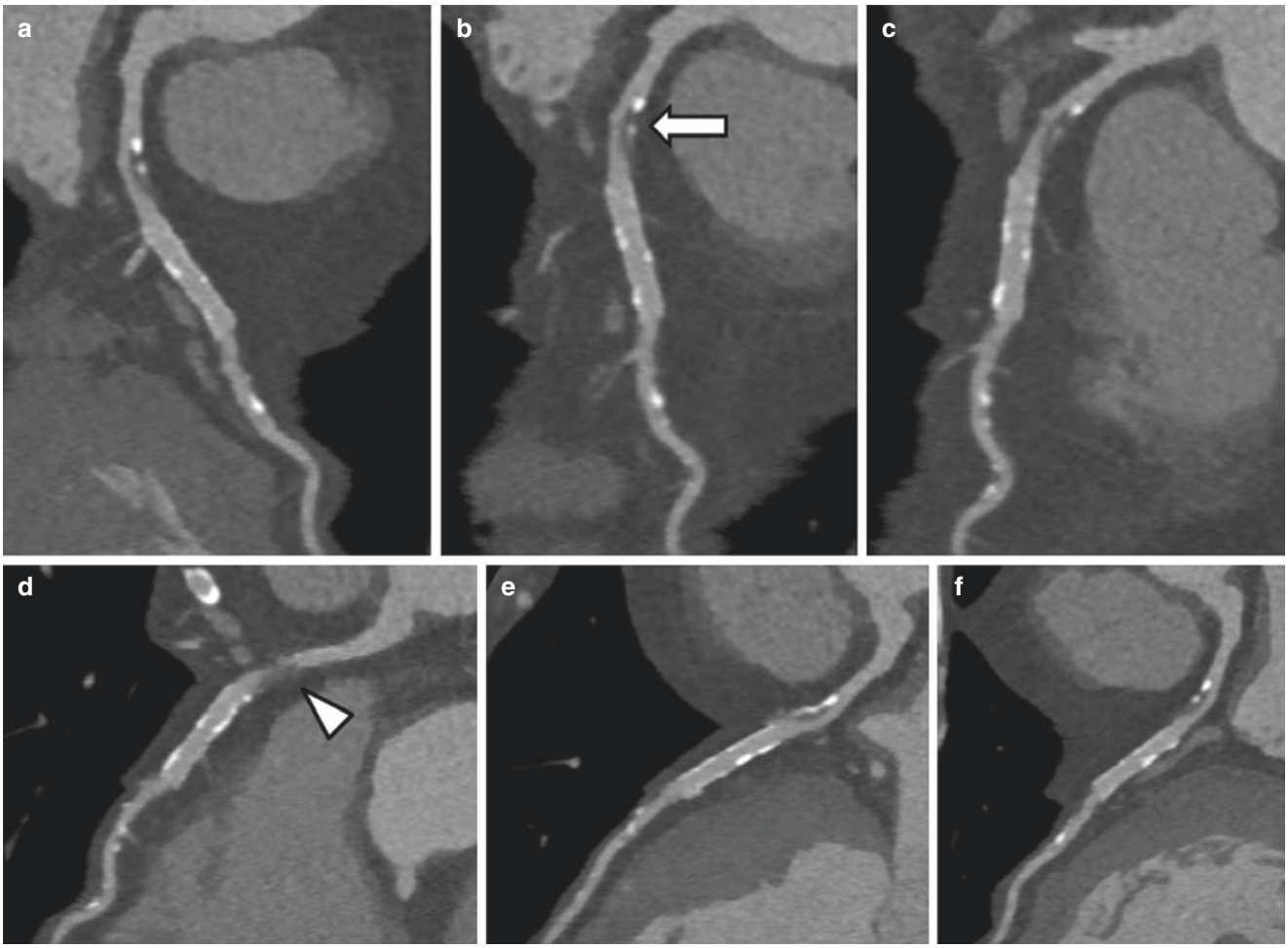

Fig. 13.6 The assessment of curved multi-planar reformat (cMPR) images from multiple views is crucial for accurate coronary artery evaluation. Varying angulations, achieved by manual swiveling around the coronary centerline, reveal different details of a coronary stenosis (*arrow*) with mixed calcified and soft-plaque of the LAD proximal to an implanted stent. Note that the severity of luminal narrowing could be over- or underestimated by only examining one cMPR image (**d**, *arrowhead*). The full extent of this mixed calcified-noncalcified plaque, and its effect on the lumen, is best understood when all different projections are considered. Figure (**d**) accentuates the noncalcified portion (*arrowhead*) and makes the stenosis appear more severe than it really is. (**a**), (**b**), (**c**), (**e**), and (**f**) demonstrate the mixed nature of the plaque and less severe stenosis

Fig. 13.7 cMPR images of a diseased LAD show the effect of adjusted window/level settings on the apparent size of calcifications within a significant stenotic lesion. Both window width decreases and level increases from image (**a**) to (**c**). The calcifications are overestimated using narrower and brighter window settings due to blooming artifacts (**c**, *arrow*). The same effect can be observed for an implanted stent (*arrowhead*). This highlights the necessity of widening preset settings for improved luminal visualization in the presence of calcified plaque or stents

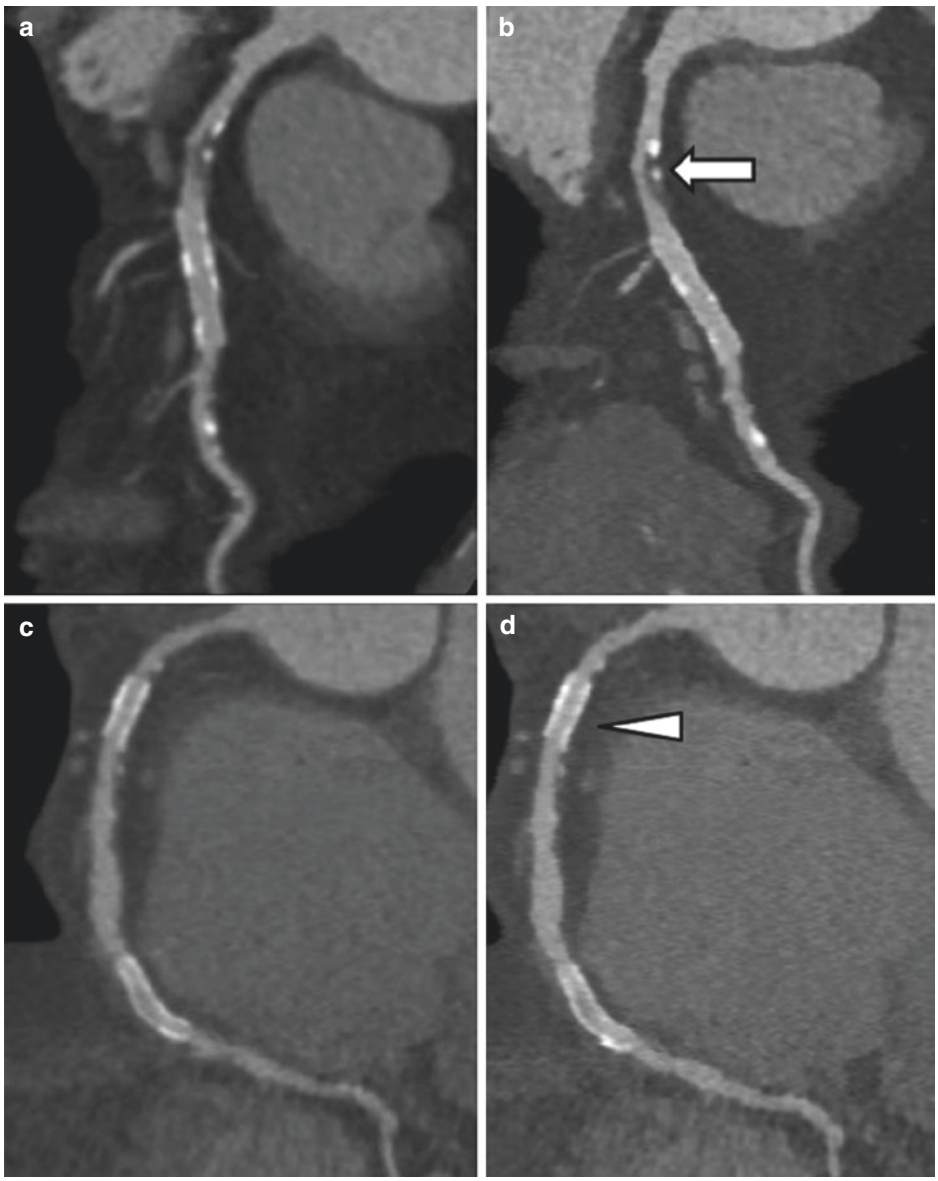

Fig. 13.8 In this patient, post-processing was performed using filtered back projection (**a** and **c**), as well as with iterative reconstruction (**b** and **d**). A mixed stenosing plaque of the LAD (*arrow*) and a coronary stent in the RCA (*arrowhead*) are more sharply depicted by means of iterative reconstruction, whereas filtered back projection images show a grainier image appearance and blurry coronary lumen

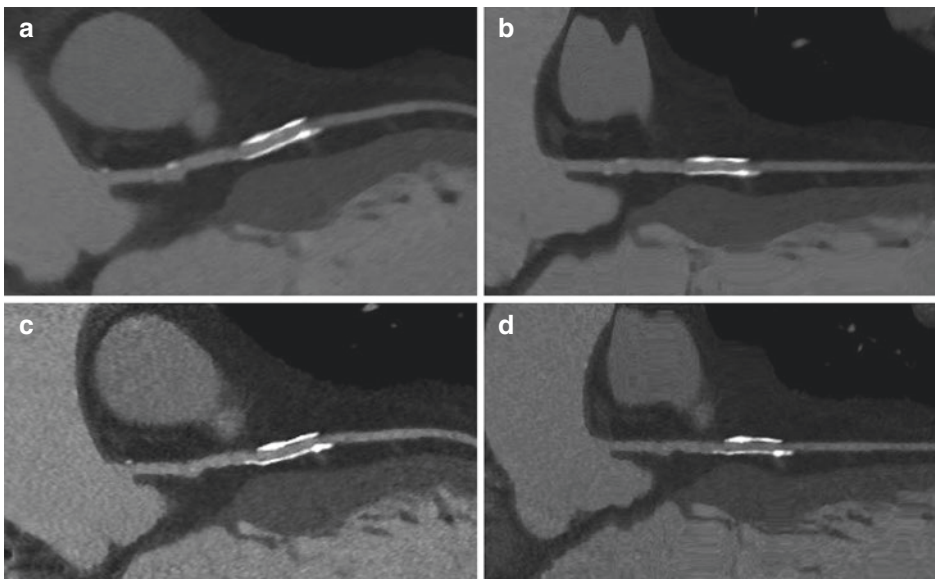

Fig. 13.9 In this patient, an LAD stent is visualized on a cMPR (**a**) and a sMPR (**b**), both of which are based on *soft tissue kernel* reconstructions. The same coronary is then depicted using a dataset reconstructed with *stent (sharp) kernel* on cMPR (**c**) and sMPR (**d**). The coronary stent is more sharply depicted by means of the stent kernel reducing blooming artifacts and increasing our ability to detect subtle intimal hyperplasia in the midportion of the stent

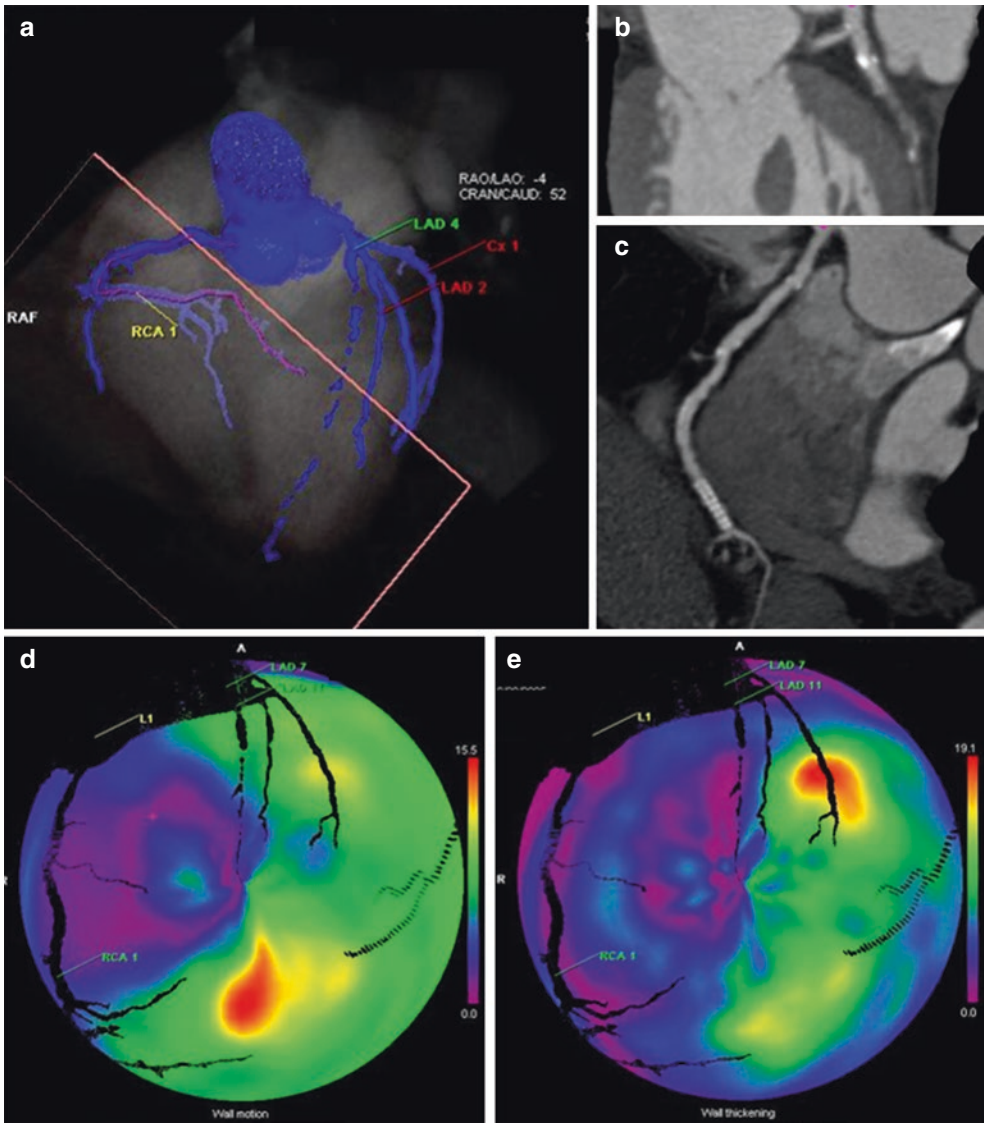

Fig. 13.10 Segmentation and evaluation of the coronary tree (**a**) of this patient revealed subtotal occlusion of the LAD (cMPR, **b**) and severely diseased, stented RCA (cMPR, **c**). By projecting the coronary tree onto polar maps of regional function obtained from the functional CT dataset (wall motion, **d**; wall thickening, **e**), the significance of coronary disease and consequent functional impairment (shown in cold colors) becomes apparent

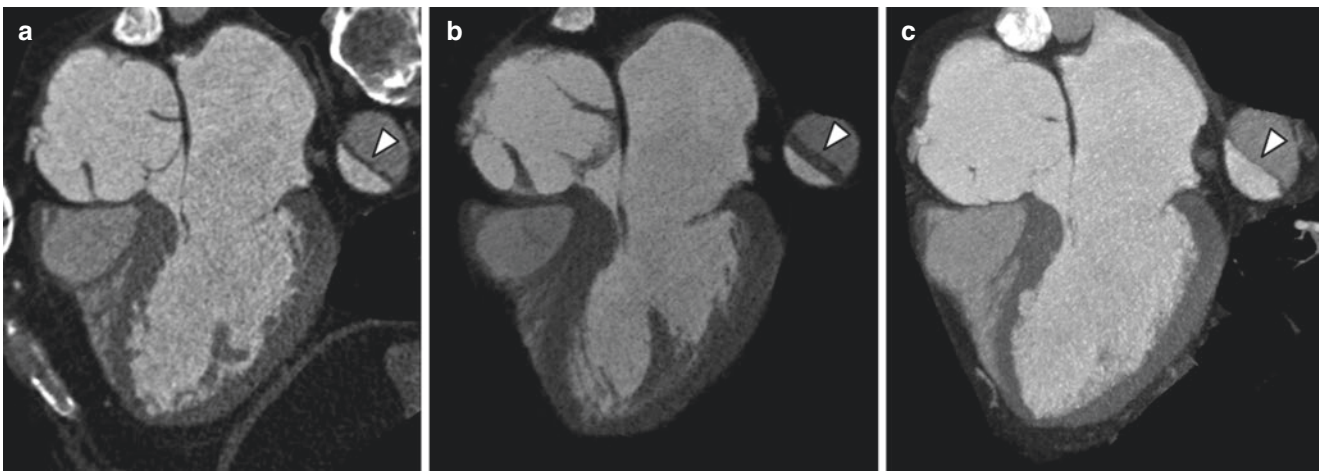

Fig. 13.11 (**a**–**c**) Three-chamber views applying MPR (0.75 mm), MINIP (10 mm), and MIP (10 mm) algorithms of the same location of a patient with aortic dissection. Note that hypoattenuating structures such as valves or dissection membranes (*arrowheads*) are best visualized with MINIP while they are almost invisible on MIP images

(see above). Some workstations will also ask for the user to mark the point of maximal stenosis in the vessel of interest. However, defining the point of maximal stenosis is often difficult due to the presence of bifurcations, calcifications, and potentially motion artifacts that may cause erroneous measurements.

Therefore, automated stenosis quantification using cardiac multi-detector CT (MDCT) data is a controversial issue, despite the fact that some investigators have shown that specialized software may be just as efficient as visual grading or invasive coronary angiography with regard to quantitative analysis [6, 7]. Many studies have demonstrated the outstanding negative predictive value of MDCT [8, 9]. However, the accurate determination of whether a stenotic lesion causes myocardial ischemia remains a challenge. Even if our images and anatomic stenosis quantification methods were impeccable, simulating the hemodynamic characteristics over a narrowed coronary is incredibly complex and is dependent on numerous additional factors beyond the extent of stenosis. For example, stenosis length, lesion geometry, blood viscosity, blood pressure, heart rate, myocardial mass, and peripheral resistance in the capillary bed are all contributing factors to determining the hemodynamic significance of a lesion. In an effort to standardize stenosis-severity reporting, a new reporting system (CAD-RADS) has just been published [10]. This system stratifies patients into risk categories and provides the probability that the source of observed chest pain is visible in the epicardial coronary arteries using CTA. The current consensus is that a radiologist – whose decision is based solely on anatomic imaging – is unable to definitively assess the hemodynamic significance of a lesion and should defer their diagnosis to the treating clinicians who should ultimately exercise clinical judgment to decide between discharge, observation, functional stress testing, and invasive catheterization.

An emerging technique of CT-derived fractional flow reserve (CT-FFR) is gaining increasing interest by using computational fluid dynamic models to quantify stenosis severity and to "simulate" how a coronary would respond to vasodilator stress testing. In general, FFR describes the decrease of blood pressure over a coronary stenosis and thus indicates the hemodynamic relevance of a lesion. Notably, current CT-FFR algorithms are based on normal static CCTA datasets and can be retrospectively employed in addition to the standard examination when more information is required [11]. To date, CT-FFR is performed mainly by outsourcing CCTA images to off-site, specialized core labs. This method takes the purely anatomic imaging a step further to virtual physiologic testing but is still highly dependent on the quality of anatomic data acquired (Fig. 13.12).

Plaque Composition Analysis

Current approaches to plaque composition analysis are still mainly investigational tools used in research projects; however, these techniques hold great promise for future CCTA evaluation and subsequent risk stratification [12]. Using threshold limits for various plaque components allows for the differentiation and volumetric determination of calcified, dominantly fibrous, and lipid-rich plaque components and provides the cardiac imager with quantitative measurements (Fig. 13.13). Analogous to the quantification of total calcified plaque burden in the context of calcium/Agatston scoring described above, these techniques may allow for more comprehensive and robust

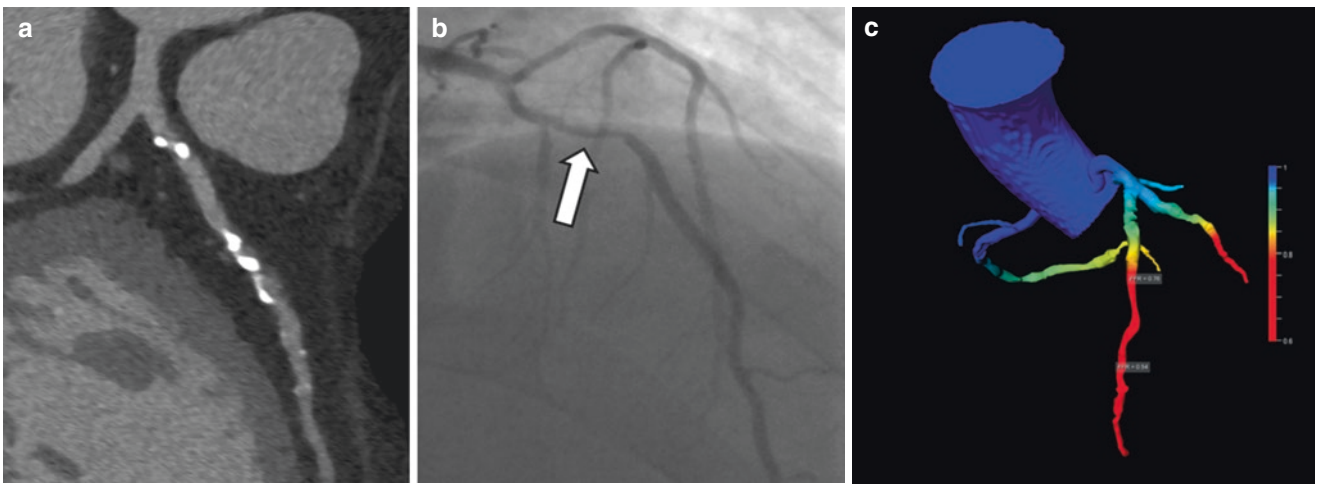

Fig. 13.12 While a stenotic calcified lesion of the LAD is clearly depicted using only cMPR images (**a**) and invasive catheterization (*arrow* in **b**), the assessment of its hemodynamic relevance remains uncertain. By means of retrospective CT-FFR calculation (**c**), this limitation can be overcome. A CT-FFR of 0.76 was shown, with almost perfect agreement to invasive FFR measurement of 0.75, an indication of a flow-restrictive coronary stenosis. (Courtesy of Christian Tesche, MD, Medical University of South Carolina, Charleston, SC, USA)

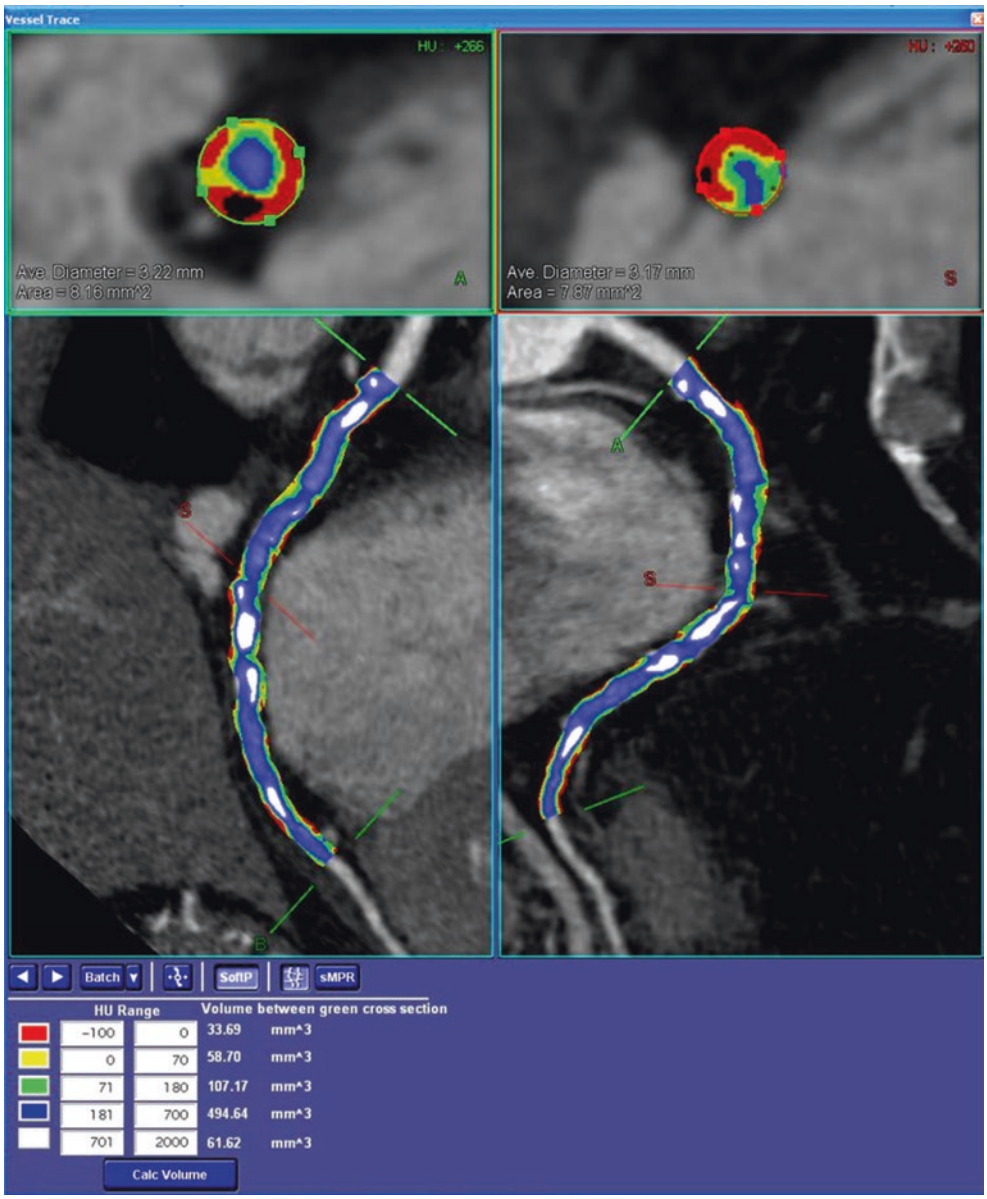

Fig. 13.13 Entire vessel plaque burden measurement using user-defined thresholds for lumen (blue), lipid-rich plaques (yellow), fibrous plaques (green), and calcifications (white). Epicardial fat and severely fatty plaques appear red

evaluation of CCTA examinations by providing quantitative results on the total lipid-rich versus fibrous plaque burden. Figure 13.13 demonstrates the processing steps of VRT, MIP, cMPR, and plaque analysis in a patient with calcified and noncalcified plaque components. Other than quantitative approaches, qualitative criteria for plaque composition and vulnerability have also been described in the literature [13].

Chamber Volumes and Ejection Fraction

The assessment of cardiac chamber dimensions and ejection fraction is an important diagnostic tool for managing patients with heart disease and making clinical decisions regarding device implantation and catheter-based or surgical interventions. Although the temporal resolution of cardiac CTA is sub-par relative to MRI or echocardiography, in patients where the first-line modalities fail or are contraindicated, CTA becomes an important surrogate to assess biventricular size and function. Various post-processing software which offer semiautomated and automated applications for volumetric analysis of cardiac chambers have become widely adopted in clinical workflows (Fig. 13.14). Most software use a combination of thresholding and contour-detection algorithms to delineate the actual complex shape of cardiac chambers, offering a tremendous advantage over conventional 2D echocardiography which mainly uses geometrical assumptions.

Quantification of ventricular chamber volumes is not only useful in assessing global systolic function and ventricular dilation but can also be utilized in assessing regurgitant frac-

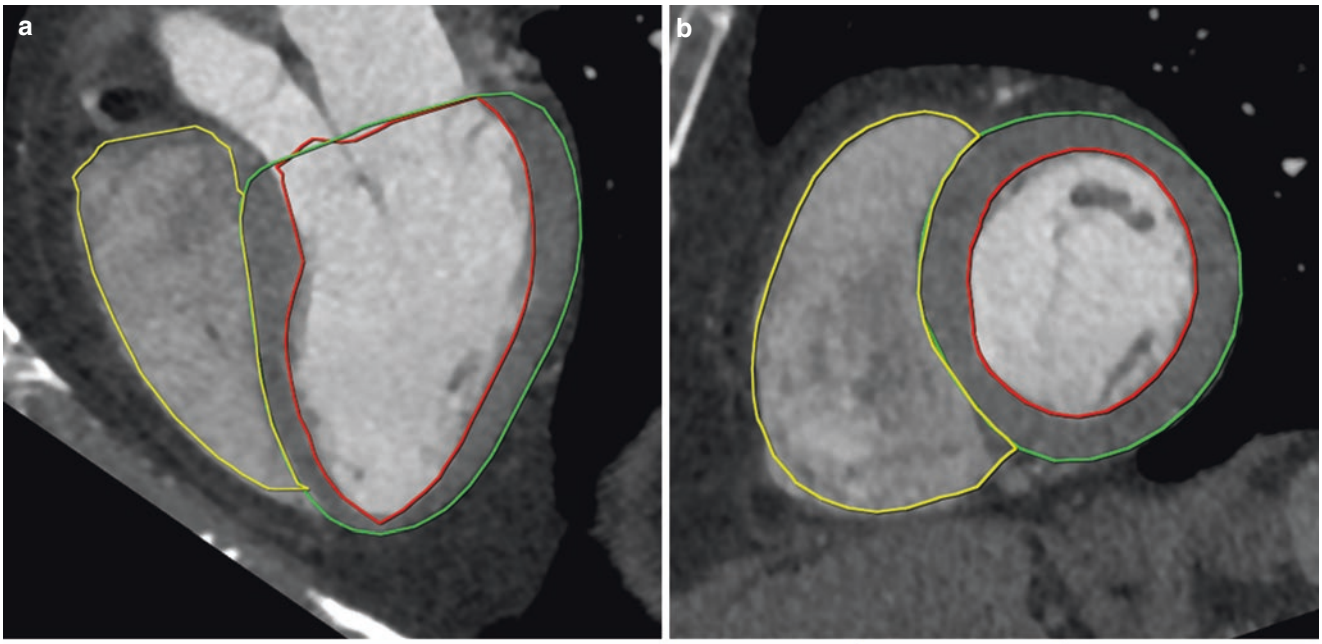

c Blood Vol. Mode

		LV	RV	Normal Values
Ejection Fraction	%	64	47	47 - 80
Myocardial Mass ED	g	119.57	-	24 - 55
Stroke Volume	ml	60.03	60.05	33 - 98
ED Volume	ml	93.92	127.64	58 - 154
ES Volume	ml	33.89	67.6	23 - 103
Cursor Volume	ml	93.92	127.64	
Cardiac Output	(l/min)	5.7	5.7	2.82 - 8.82

Height:	165	cm	5	ft	5	in	Sex: Female
Weight:	75	kg	165	lbs			BSA / m² 1.85

Fig. 13.14 Myocardial function analysis. Long- (**a**) and short-axis (**b**) views of the heart showing the segmentation of the right ventricle (yellow line) and left ventricle (red and green lines) for function analysis. Subsequently, a table with the different volumetric values is generated (**c**), providing the cardiac imager with quantitative data to assess global cardiac function, myocardial mass, and ventricular volumes

tion or pulmonic to systemic flow (Qp/Qs) in patients with valve disease or shunts.

As with any other post-processing technique, there are certain caveats one should bear in mind before "blindly" accepting the automatically generated results. The data are only as good as the source images, and the results will be influenced by overall image quality, i.e., temporal resolution, partial coverage of the cardiac cycle, signal-to-noise and contrast-to-noise relationships, streak artifacts from devices, motion artifacts, misregistrations due to arrhythmia, or patient motion. Moreover, erroneous segmentation of the chamber vs. myocardium, inclusion of atria or outflow tracts, and the faulty delineation of valve levels can all lead to an incorrect estimation of cardiac volumes (Fig. 13.15).

Assessment of the Myocardium, Regional Function, and Epicardial Fat

Hypertrophic cardiomyopathy, hypertension, and aortic stenosis are the most common causes of myocardial "overgrowth." By delineating endo- and epicardial contours, the total left ventricular myocardial mass can be determined, which can be helpful to assess disease severity and prognosis. If the contouring is performed for both end-diastole and end-systole, objective and quantitative parameters of regional function can be obtained (such as wall thickening, wall motion, segmental ejection fraction), which may help in identifying vessel territories with impaired blood supply (Fig. 13.16). However, in routine clinical practice, the traditional subjective, visual inspection of regional wall motion

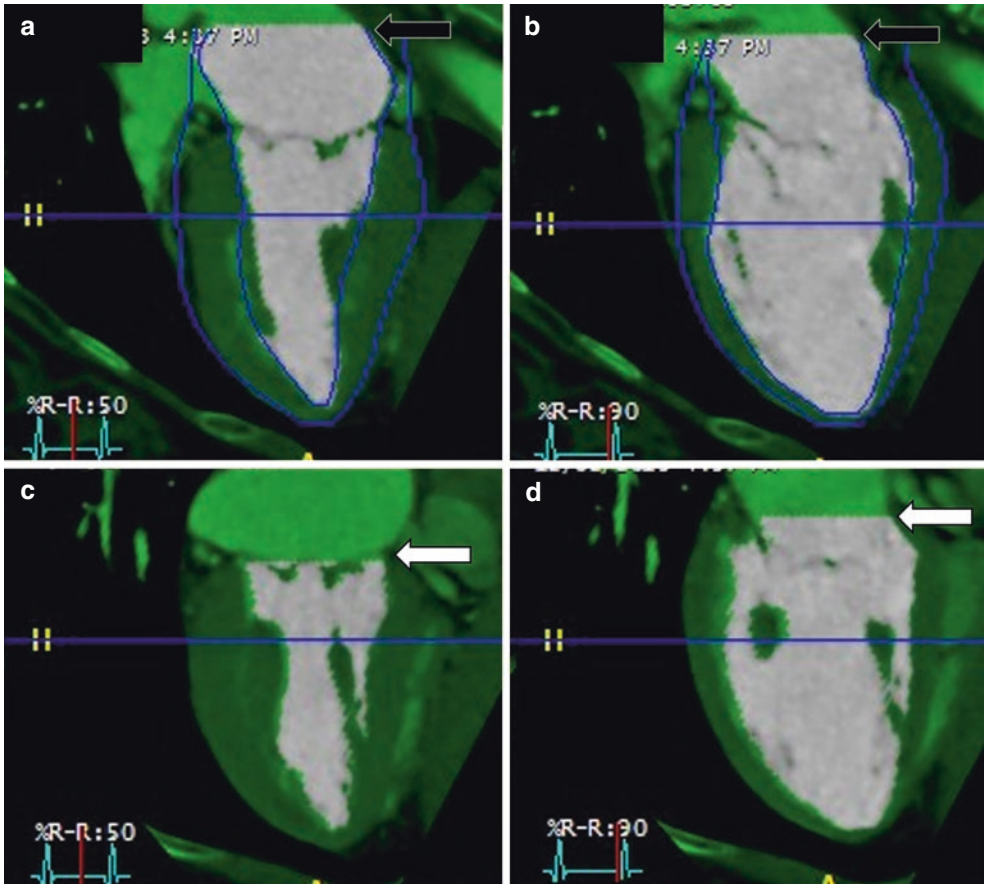

Fig. 13.15 It is crucial to visually assess the segmentation provided by automated software algorithms to avoid erroneous functional measurements. Automatically segmented images are demonstrated in systole (**a** and **c**) and diastole (**b** and **d**). In this particular case, the initial segmentation (**a** and **b**) included large parts of the left atrium (*black arrows*), and this leads to marked underestimation of the ejection fraction (38%). After manual adjustment of the mitral valve level (*white arrows*), the ejection fraction was calculated to be 70%, within normal range

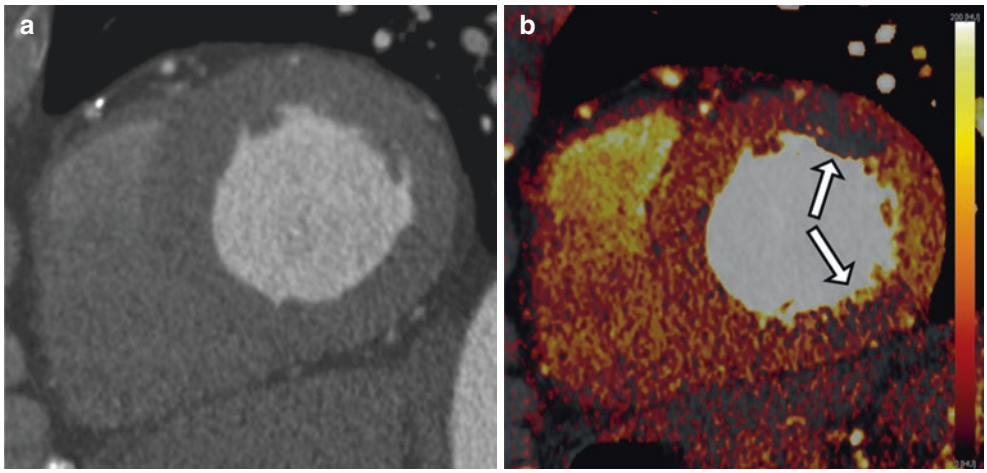

Fig. 13.16 Dual-energy CT myocardial iodine maps. This figure shows a short-axis MPR image of the heart (**a**) where the myocardium appears normal. Post-processing of the dual-energy CT dataset allowed the generation of an iodine map of the myocardium (**b**) which helped detect areas of subtle hypoperfusion (*arrows*)

remains the standard method of choice and is performed using dedicated cardiac planes in the long and short axis, as discussed above.

While contrast-enhanced MRI remains the gold standard for myocardial viability assessment, the phenomenon of delayed hyperenhancement has also been described as useful in delineating subacute infarcts and fibrosis with cardiac CT [14, 15]. Extracellular volume fraction (ECVF) calculations can also be performed to quantify and assess myocardial fibrosis [16]. ECVF is calculated based on attenuation characteristics on unenhanced and contrast-enhanced CT images, taking the patient's hematocrit into account. These techniques are discussed in more detail elsewhere in this book, but are not currently part of routine clinical evaluation.

Several studies have quantified epicardial fat in both semi-automated and automated fashions and suggested an added value for predicting patient outcome and risk stratification [17]. The most sophisticated, cutting-edge post-processing to date is using CTA-derived data to depict infiltrating myocardial fat and delayed hyperenhancing infarcts/fibrosis fused with electrophysiological mapping data [18]. This method holds the promise to potentially guide radiofrequency ablation for ventricular or atrial arrhythmias.

Dual-Energy CT/Perfusion Imaging

Another rapidly growing field in cardiac CT is the development of gated dual-energy cardiac scans, which is further detailed in other chapters of this book. One method to generate these images is to use two different tube currents (e.g., 80 kV and 140 kV) in two tubes of a dual-source scanner, which acquires two accurately co-registered image sets with a temporal resolution of a single-source 64-slice CT scanner. In many cases, this is sufficient for simultaneous CCTA. The mAs setting is usually adjusted so that the noise levels are similar in the two image sets. Thus, the trade-off is temporal resolution (for instance, 165 ms vs. 83 ms), but the benefit is the ability to identify, localize, and quantify the amount of iodine present in varying tissues. This value is correlated with tissue perfusion, which can be quantified in mg/ml, and may be beneficial in cases of suspected perfusion deficits and myocardial tissue characterization. Using dedicated filtering (D kernels) for reconstruction is essential, and various color codes can be used to visualize hypoperfused regions of the myocardium (Fig. 13.17).

CT myocardial perfusion during vasodilator stress, based on principles similar to MRI-based first-pass perfusion, is yet another exciting field emerging and receiving growing acceptance from the radiology community. One approach provides a "subtraction" dataset, depicting areas of differential perfusion between rest and stress datasets (Fig. 13.17). While other chapters in this book will discuss the various ways of acquiring these images, we wanted to include an example of a post-processed dataset where myocardial blood flow is quantitatively mapped over time with dynamic, also known as time-resolved, perfusion CT technique (Fig. 13.18).

Fusion with Other Modalities

The volumetric data from cardiac CTA is also being used to enhance visualization and provide guidance for several additional modalities. While a comprehensive overview of this topic is beyond the scope of our current chapter, CT has been fused with nuclear medicine SPECT or PET myocardial perfusion imaging [19], where the power of anatomic detail with CT is paired with the physiologic information from SPECT or PET. CT has also been instrumental in the developments of electrophysiology, where surface mapping fused with CT data helps identify the substrate for ventricular arrhythmia and 3D visualization of pulmonary venous anatomy can aid in radiofrequency ablations for atrial fibrillation [20].

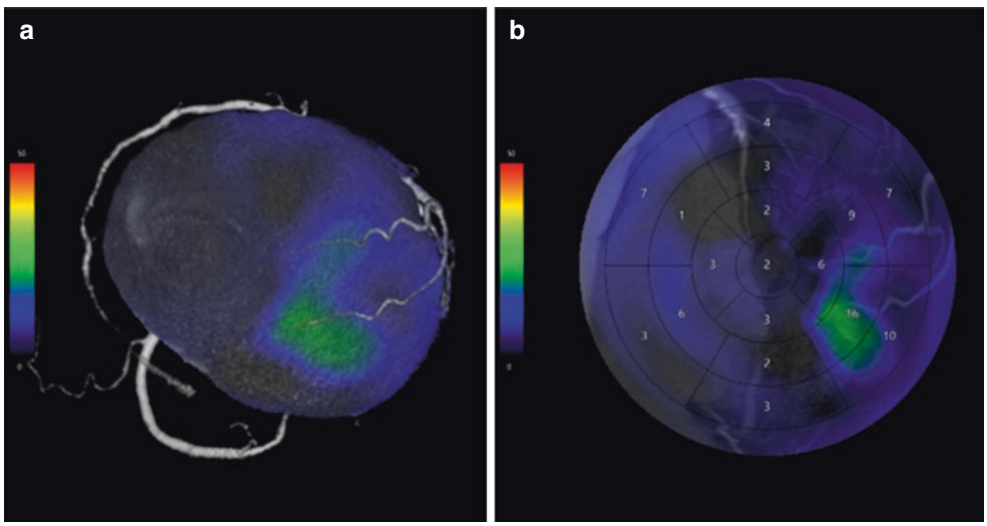

Fig. 13.17 Myocardial stress perfusion images can be subtracted from the rest dataset. The resulting 3D VRT (**a**) and superimposed polar map (**b**) show green areas of stress-induced ischemia. (Courtesy of FUJIFILM Medical Systems USA, Inc.)

Outsourcing, Web Clients, and the "Cloud"

Outsourcing of the post-processing steps – whether to the well-trained CT technologist in the department or to dedicated 3D-workstation experts overseas – has become somewhat of a routine in some centers. This approach is meant to speed up interpretation by providing the interpreting physician with snapshots of MIPs, 3D VRTs, and cMPRs of the heart and allowing them to "flip through" the pictures, which clearly has advantages in terms of workflow and throughput. Still, we firmly believe that in complex or challenging cases, the ability to interact with the post-processed dataset firsthand is crucial for avoiding errors in interpretation. The clinician needs to be able to adjust the window/level settings, rotate the 3D VRT heart, swivel around the entire vessel when using cMPR, and adjust the thickness of a MIP or a MINIP to fully assess and understand the true extent of the pathology. Thus, interpreters of cardiac CT need to train themselves and become comfortable with applying these techniques to allow for a comprehensive analysis of CT images of the heart (Fig. 13.19). A great aid for this are "web-client"-based systems, allowing simultaneous use of a 3D workstation by multiple users from anywhere, at any time, provided they have a computer and a reasonable internet connection. In addition, ongoing and future research is needed to investigate the clinical value and cost-effectiveness of various existing visualization and quantification techniques. Workflow optimization remains a major concern as we strive to adopt these novel approaches into the routine clinical workflow of cardiac imaging.

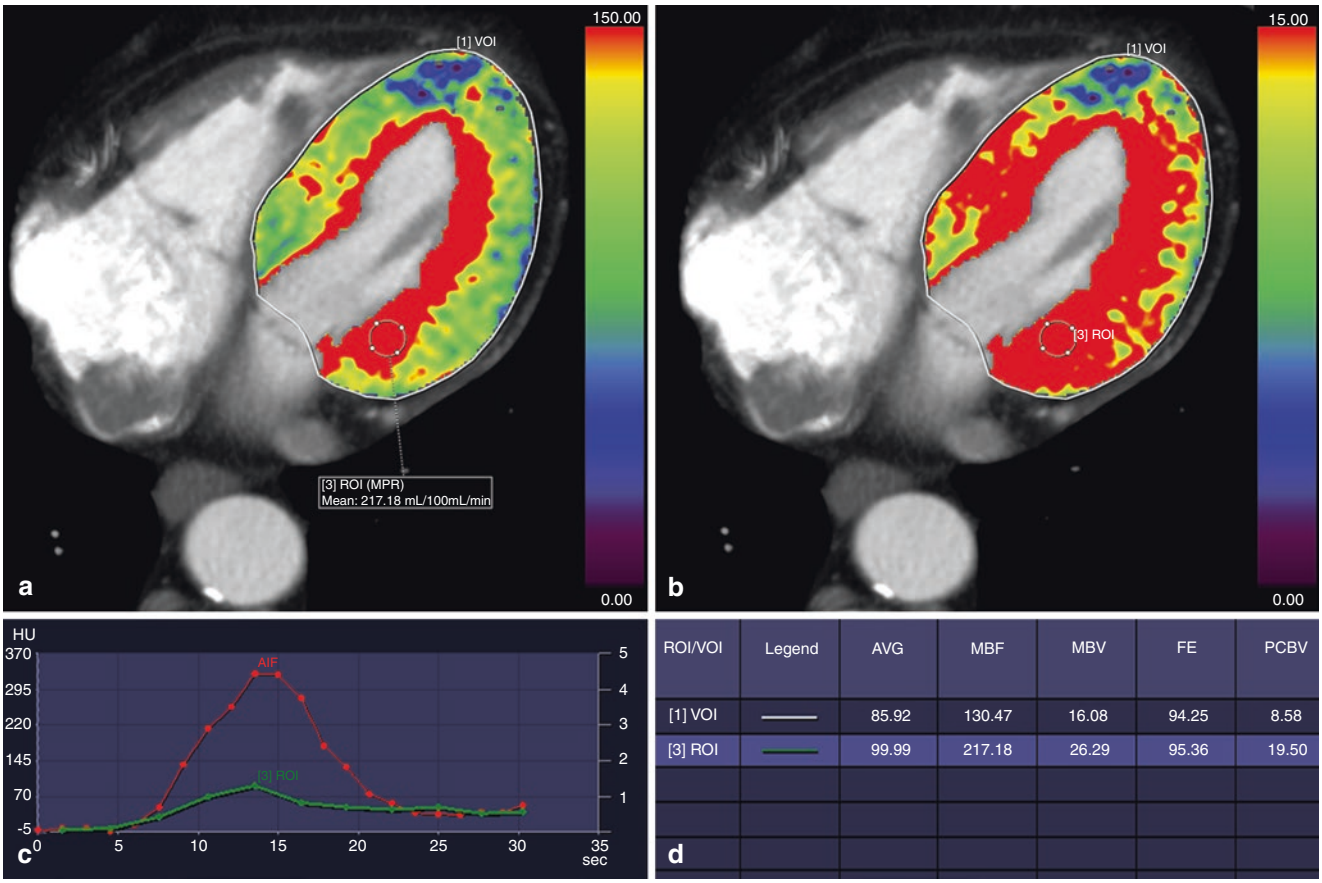

Fig. 13.18 Quantitative myocardial perfusion analysis. Color-coded maps of myocardial blood flow (**a**) and myocardial blood volume (**b**) illustrating myocardial perfusion. Note the apical area of hypoperfusion (blue area). ROIs can be placed to generate arterial input functions (AIF) and perfusion curves (**c**), where each point indicates the attenuation during the dynamic sequential image acquisition. As a result, a table of objective calculated values (**d**), such as myocardial blood flow (MBF) and myocardial blood volume (MBV), can be generated for quantitative myocardial perfusion analysis

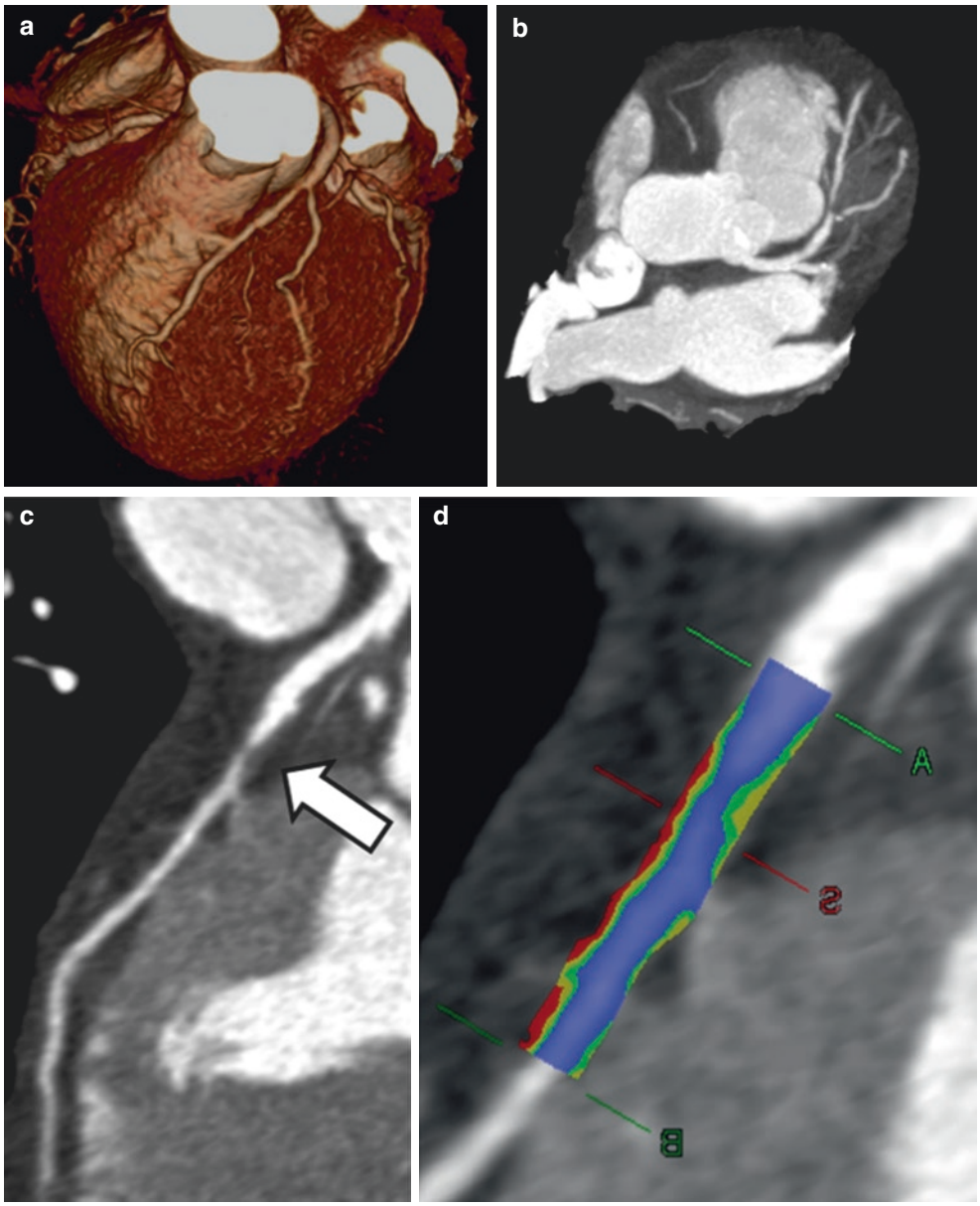

Fig. 13.19 Working up a case: 3D VRT showed a suspicious bifurcation of the LAD and the first diagonal (**a**). MIP showed the presence of mixed, calcified and noncalcified components (**b**). cMPRs of the LAD (**c**) and color-coded plaque analysis (**d**) showed the lipid-rich nature of the noncalcified portions of the lesion

References

1. Fishman EK, Ney DR, Heath DG, et al. Volume rendering versus maximum intensity projection in CT angiography: what works best, when, and why. Radiographics. 2006;26:905–22.
2. van Ooijen PMA, Ho KY, Dorgelo J, Oudkerk M. Coronary artery imaging with multidetector CT: visualization issues. Radiographics. 2003;23:e16.
3. Geyer LL, Glenn GR, De Cecco CN, et al. CT evaluation of small-diameter coronary artery stents: effect of an integrated circuit detector with iterative reconstruction. Radiology. 2015;276:706–14.
4. Hecht HS. Coronary artery calcium scanning. JACC Cardiovasc Imaging. 2015;8:579–96.
5. Busch S, Johnson TRC, Nikolaou K, et al. Visual and automatic grading of coronary artery stenoses with 64-slice CT angiography in reference to invasive angiography. Eur Radiol. 2007;17:1445–51.
6. Arbab-Zadeh A, Hoe J. Quantification of coronary arterial stenoses by multidetector CT angiography in comparison with conventional angiography. JACC Cardiovasc Imaging. 2011;4:191–202.
7. Boogers MJ, Schuijf JD, Kitslaar PH, et al. Automated quantification of stenosis severity on 64-slice CT. JACC Cardiovasc Imaging. 2010;3:699–709.
8. Stein PD, Yaekoub AY, Matta F, Sostman HD. 64-slice CT for diagnosis of coronary artery disease: a systematic review. Am J Med. 2008;121:715–25.
9. Janne d'Othée B, Siebert U, Cury R, et al. A systematic review on diagnostic accuracy of CT-based detection of significant coronary artery disease. Eur J Radiol. 2008;65:449–61.
10. Cury RC, Abbara S, Achenbach S, et al. CAD-RADS™: coronary artery disease – reporting and data system. J Am Coll Radiol. 2016;13(12 Pt A):1458–1466.e9.
11. Gaur S, Taylor CA, Jensen JM, et al. FFR derived from coronary CT angiography in nonculprit lesions of patients with recent STEMI. JACC Cardiovasc Imaging. 2016;10:424–33.

12. Gitsioudis G, Schüssler A, Nagy E, et al. Combined assessment of high-sensitivity troponin T and noninvasive coronary plaque composition for the prediction of cardiac outcomes. Radiology. 2015;276:73–81.
13. Maurovich-Horvat P, Schlett CL, Alkadhi H, et al. The napkin-ring sign indicates advanced atherosclerotic lesions in coronary CT angiography. JACC Cardiovasc Imaging. 2012;5:1243–52.
14. Lardo AC. Contrast-enhanced multidetector computed tomography viability imaging after myocardial infarction: characterization of myocyte death, microvascular obstruction, and chronic scar. Circulation. 2006;113:394–404.
15. Gerber BL. Characterization of acute and chronic myocardial infarcts by multidetector computed tomography: comparison with contrast-enhanced magnetic resonance. Circulation. 2006;113:823–33.
16. Bandula S, White SK, Flett AS, et al. Measurement of myocardial extracellular volume fraction by using equilibrium contrast-enhanced CT: validation against histologic findings. Radiology. 2013;269:396–403.
17. Spearman JV, Meinel FG, Schoepf UJ, et al. Automated quantification of epicardial adipose tissue using CT angiography: evaluation of a prototype software. Eur Radiol. 2014;24:519–26.
18. Truong QA, Thai W, Wai B, et al. Myocardial scar imaging by standard single-energy and dual-energy late enhancement CT: comparison with pathology and electroanatomic map in an experimental chronic infarct porcine model. J Cardiovasc Comput Tomogr. 2015;9:313–20.
19. Thilo C, Schoepf UJ, Gordon L, et al. Integrated assessment of coronary anatomy and myocardial perfusion using a retractable SPECT camera combined with 64-slice CT: initial experience. Eur Radiol. 2009;19:845–56.
20. Cochet H, Dubois R, Sacher F, et al. Cardiac arrhythmias: multimodal assessment integrating body surface ECG mapping into cardiac imaging. Radiology. 2014;271:239–47.